International Journal of Nanomedicine

Dovepress
Taylor & Francis Group

Open Access Full Text Article

ORIGINAL RESEARCH

Tailoring Polydopamine Nanoparticle Size Through Synthesis Conditions and Defining Their Antioxidant and Neuroprotective Efficacy

Qianqian Huang, Junbo Zou, Fei Luan, Yajun Shi

Shaanxi Key Laboratory of Chinese Medicine Fundamentals and New Drugs Research, School of Pharmacy, Shaanxi University of Chinese Medicine, Xianyang, Shaanxi, 712046, People's Republic of China

Correspondence: Yajun Shi, Email 2051004@sntcm.edu.cn

Introduction: Oxidative stress is a central pathological process in neurodegenerative diseases, driving the need for neuroprotective agents capable of scavenging reactive oxygen species (ROS). Polydopamine nanoparticles (PDA) hold promise due to their antioxidant properties, but their biomedical application has been limited by challenges in achieving precise size control.

Methods: We established a controllable synthesis of PDA by systematically optimizing the alkaline polymerization parameters, including pH, temperature, and reaction time. We also evaluated their antioxidant and neuroprotective efficacy.

Results: This approach yielded monodisperse, spherical PDA with a diameter of approximately 60 nm. The synthesized NPs exhibited potent ROS-scavenging capacity, effectively protected neuronal cells from oxidative stress, and promoted microglial polarization from a pro-inflammatory M1 to an anti-inflammatory M2 phenotype.

Discussion: Our study not only systematically establishes the technical parameters for the controlled preparation of PDA but also elucidates the dual mechanisms of antioxidant activity and immunomodulation. Those results demonstrate their potential as efficient neuroprotective nanotherapeutics, while providing a solid theoretical and experimental foundation for related drug development.

Keywords: polydopamine, particle size, react conditions, reactive oxygen species scavenge, microglial polarization

Introduction

Oxidative stress is a central pathological process in neurodegenerative diseases.[1,2] Mechanistically, excessive reactive oxygen species (ROS) damage neuronal lipids, proteins, and DNA, leading to mitochondrial dysfunction and cell death, while also triggering a neuroinflammatory response mediated by microglial activation.[1,3] Activated microglia may polarize toward a pro-inflammatory M1 phenotype that exacerbates neuronal injury or an anti-inflammatory M2 phenotype that supports repair. Sustained M1 activation creates a vicious cycle of oxidative stress and inflammation that accelerates disease progression.[4] Therefore, disrupting this cycle using agents that simultaneously scavenge ROS and modulate microglial polarization represents a promising therapeutic strategy.

The development of nanotherapeutics capable of efficiently scavenging excess ROS is a cutting-edge frontier in neuroprotection research.[5–7] Key challenges in neuro-nanomedicine include achieving sufficient brain biodistribution, enabling cell-specific delivery, and ensuring long-term biosafety.[8] Inspired by the adhesive proteins in mussel byssi, polydopamine nanoparticles (PDA) have emerged as novel biomimetic polymers, garnering significant attention in materials science and biomedicine in recent years.[9,10] Their diverse and straightforward synthesis methods, often under mild conditions, yield materials with remarkable properties, including excellent photothermal conversion efficiency,[11,12] robust surface adhesion,[13,14] and potential chemical reactivity.[15] Notably, their significant antioxidant activity, stemming from abundant catechol groups in their molecular structure, enables effective ROS scavenging.[16–18] Owing to their biocompatibility and biodegradability, PDA regarded as highly promising nanomaterials for neuroprotection.

https://doi.org/10.2147/IJN.S581479
Received: 14 November 2025
Accepted: 16 January 2026
Published: 27 January 2026

Although the synthesis of PDA appears straightforward, their polymerization process is complex and susceptible to various factors, allowing precise control over the morphology, size, and monodispersity of the resulting particles. For NPs, size is one of the most critical physical parameters, directly influencing the specific surface area, in vivo distribution, tissue penetration capability, and, ultimately, biological effects.[19–21] A size around 50–60 nm is particularly favorable for nanomedicine, offering an optimal balance between circulation time, cellular uptake, and potential for BBB translocation.[20,22] Therefore, achieving a controllable PDA size is a prerequisite for translating them from basic research to application. Currently, the most common synthetic method involves self-polymerization under alkaline conditions. However, systematic studies on how synthesis parameters such as reactant concentration, temperature, and reaction time affect the production of monodisperse PDA with a uniform size remain insufficient. The principles and mechanisms governing size control require in-depth exploration.

This study aimed to investigate the effects of different reaction conditions in alkaline polymerization on the size of the synthesized PDA, establish a technical pathway for their controlled preparation, and systematically evaluate their neuroprotective potential. First, we systematically examined the influence of key parameters, including reaction temperature, duration, and initial dopamine concentration, on the final size and distribution of PDA, enabling size control from the synthesis outset. Subsequently, from a series of particles of different sizes, we identified the ideal candidate for brain delivery based on their dimensions, dispersity, and stability. Following the acquisition of the target NPs, we conducted comprehensive characterization and performed in-depth biological functional evaluations. We assessed their cell viability and investigated their cellular uptake. Their antioxidant activity was evaluated using ROS clearance assays, and their neuroprotective effects were validated in neuronal oxidative stress models induced by hydrogen peroxide, alongside an examination of their ability to modulate microglial polarization. This study not only provided crucial data for the controlled preparation of PDA via the alkaline method but, more importantly, established a solid theoretical and experimental foundation for developing efficient PDA-based neuroprotective nanoformulations through an integrated research strategy.

Materials and Methods

Materials

Dopamine hydrochloride was purchased from Sigma–Aldrich (St. Louis, MO, USA). 2',7'-Dichlorodihydrofluorescein diacetate (DCFH-DA) was obtain from Bide Pharmatech Co., Ltd. (Shanghai, China). Cy5-NH_2 was purchased from Dalian Meilun Biotechnology Co. Ltd. (China). Complete RPMI-1640, Dulbecco's modified Eagle's medium (DMEM), trypsin-EDTA solution, and fetal bovine serum (FBS) were purchased from Gibco (USA). Anti CD206 and CD86 antibody were obtained from Proteintech Group Inc. (Wuhan, China). All chemicals used were of analytical or reagent grade. The PC-12 and BV2 cell lines were obtained from the Cell Bank of the Chinese Academy of Sciences (Shanghai, China). Cells were cultured in complete RPMI-1640 or DMEM containing 10% FBS, 100 U/mL penicillin-streptomycin (P/S), and maintained in incubator under a condition of 37°C and 5% CO_2.

An electronic analytical balance (BSA224S, Sartorius, Germany), ultrapure water conductivity meter (UPT-II-10T, China), laser particle size/zeta potential analyzer (Size Nano ZS90, Malvern, UK), microplate reader (Varioskan Flash, Thermo Scientific, USA), ultraviolet spectrophotometer (GENESYS 180, Thermo Scientific, USA), transmission electron microscope (TEM H-600 Hitachi, Shimadzu, Japan), fluorescence microscope (Thunder DMi8, Leica, Germany), flow cytometer (NovoCyte Advanteon, Agilent, USA), and cell incubator (CCL-170B-8, ESCO, Singapore) were used.

Effect of Reaction Conditions on PDA Size

PDA were synthesized via self-polymerization of dopamine hydrochloride under alkaline conditions in a Tris buffer system. To screen for PDA with an optimal particle size, the influence of different reaction conditions (pH, temperature, and time) on the PDA size was investigated.

Reaction pH

To examine the effect of reaction pH on the size of synthesized PDA, prepared 50 mM Tris solutions were adjusted to different pH values, specifically pH 8, 9, 10, 11, 11.5, and 12. The pH-adjusted Tris buffer was placed in a round-bottom flask positioned in a constant-temperature stirring water bath, with the reaction temperature fixed at 37°C, and the stirring

speed set to 420 rpm. After temperature stabilization, precisely weighed dopamine hydrochloride was added to achieve a final concentration of 1 mg/mL. The reaction was allowed to proceed for 2 h under open air conditions. The resulting solution was then centrifuged and purified to obtain PDA, which were stored at 4°C for subsequent use.

Reaction Temperature

To investigate the impact of the reaction temperature on PDA size, the reaction pH was fixed at 11.5. The pH-adjusted 50 mM Tris buffer was added to a round-bottom flask in a constant-temperature stirring water bath at reaction temperatures set to 25°C, 37°C, and 50°C, respectively. The stirring speed was 420 rpm. After temperature equilibration, precisely weighed dopamine hydrochloride was added to a final concentration of 1 mg/mL and the open-air reaction was allowed to proceed for 2 h. The resulting PDA were collected via centrifugation, purified, and stored at 4°C.

Reaction Time

To assess the effect of reaction time on NP size, the reaction pH was fixed at 11.5 and the temperature at 37°C. The pH-adjusted Tris buffer was placed in a round-bottomed flask in a constant-temperature stirring water bath, set to 37°C and 420 rpm. Following temperature stabilization, precisely weighed dopamine hydrochloride was added (final concentration, 1 mg/mL). The open-air reaction was carried out for 1, 2, 4, and 12 h. The resulting NPs were subsequently centrifuged, purified, and stored at 4°C.

Purification and Quantification of PDA

The standardized synthesis procedure for PDA was based on previously established optimized reaction conditions. The resulting reaction solution was aliquoted into 1.5 mL microcentrifuge tubes. Purification was performed via centrifugation using a high-speed refrigerated centrifuge at 4°C and 12,000 rpm for 15 min. The supernatant was carefully removed, and the pellet was resuspended in ultrapure water. The centrifugation and washing cycle was repeated twice more, for a total of three washes to obtain purified PDA. For quantification, a portion of the purified PDA suspension was lyophilized to determine NP mass. Another aliquot from the same purification batch was serially diluted to obtain solutions of varying concentrations and the absorbance of these solutions was measured at 450 nm. A standard curve was constructed by plotting the measured absorbance values against the corresponding NP masses determined for the lyophilized samples.

NPs Characterization

An appropriate volume of the purified NP suspension was diluted for subsequent analyses. The hydrodynamic diameter and zeta potential of the synthesized NPs were determined using a laser diffraction particle size/zeta potential analyzer. Another aliquot of the purified suspension was diluted and prepared for TEM to examine its morphology.

Synthesis of Fluorescently Labeled NPs

To enable subsequent visualization and quantification of NP distribution, the NPs were fluorescently labeled. Cy5-NH_2 was dissolved in dimethyl sulfoxide (DMSO) at a concentration of 10 mg/mL to prepare a stock solution. Under alkaline conditions (pH > 8.5), Cy5-NH_2 solution was mixed with PDA suspension (0.4 mg/mL) at a volume ratio of 1:100. The reaction proceeded in a constant-temperature water bath at 25°C with stirring at 450 rpm for 24 h. The resulting product was then collected and subjected to repeated centrifugation (15 min per cycle at 12,000 rpm and 4°C) using ultrapure water to remove any unreacted Cy5 molecules. The reaction scheme between the amino and catechol groups on the PDA surface is illustrated in Figure 1.

Cellular ROS Scavenging Assay

Flow Cytometric Analysis

PC-12 cells were seeded into 12-well plates at a density of 1×10^5 cells/well. After 24 h, the culture medium was replaced with fresh medium containing PDA (100 μg/mL) and the cells were incubated for another 24 h at 37°C. Subsequently, the medium was replaced with a solution containing 50 μM tert-butyl hydroperoxide (TBH) in culture medium, and

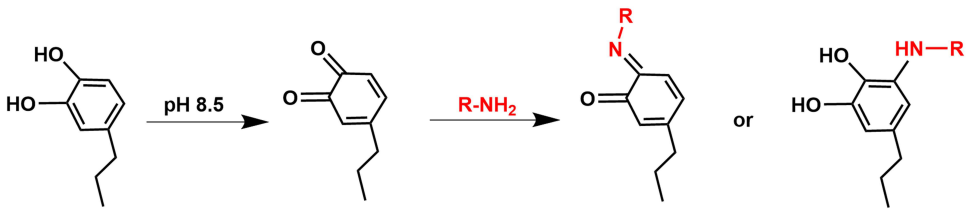

Figure 1 The Siciff base and/ Michael addition reaction of amino group with the catechol of PDA. The parts marked in red are the reaction groups.

incubation continued for 6 h at 37°C. Following TBH treatment, the medium was aspirated and incubated with serum-free medium containing 10 μM DCFH-DA for 30 min at 37°C. The cells were collected for immediate analysis via flow cytometer.

Fluorescence Microscopy Imaging

For fluorescence microscopy analysis, PC-12 cells were seeded at a density of 1×10^5 cells per well on glass coverslips in 12-well plates. The subsequent treatment steps, including PDA incubation, TBH exposure, and DCFH-DA loading, were identical to those described for the flow cytometry experiment. After incubation with DCFH-DA, the cells were fixed with 4% paraformaldehyde and stained with DAPI (1 μg/mL) for 5 min. The cells were visualized and imaged using a fluorescence microscope.

Microglial Polarization Assay

BV2 cells were seeded on glass coverslips placed in 12-well plates at a density of 3×10^4 cells per well. The cells were cultured until they reached 70–80% confluence. The culture medium was then replaced with fresh medium containing PDA (100 μg/mL), and the cells were incubated for 24 h. After washing with PBS, the cells were exposed to culture medium containing 50 μM TBH for 6 h. Following stimulation, the cells were fixed with 4% paraformaldehyde, permeabilized with PBS containing 0.5% Tween 20, and blocked with 5% goat serum for 1 h at room temperature. The cells were then incubated overnight at 4°C with primary antibodies (CD86, 1:200 dilution; CD206, 1:500 dilution). The next day, the cells were incubated with Cy3-conjugated goat anti-rabbit secondary antibody (1:200 dilution) for 1.5 h at room temperature. After stained with DAPI for 5 min, the cells were observed and imaged using a fluorescence microscope.

Statistical Analysis

Statistical analyses were performed using GraphPad Prism software (version 9.3.1, CA). Data from at least three independent experiments are expressed as mean ± standard deviation (SD). For comparisons among multiple groups, the one-way ANOVA with the Tukey's or Dunnett's test was performed. A significance level of $P<0.05$ indicated a statistically significant difference. $*P<0.05$, $**P<0.01$, and $***P<0.001$.

Results

Screening of PDA Size

Effect of Reaction pH

At a reaction temperature fixed at 37°C and a reaction time set at 2 h, the hydrodynamic diameter of PDA progressively decreased as the pH increased. At a pH of 8, the particle size was approximately 350 nm. When the pH increased to 10, the diameter decreased to approximately 160 nm. Further increase to pH 11 yielded particles of approximately 90 nm. Notably, at pH values exceeding 12, no NP formation was observed, likely because of the excessively strong alkaline conditions. As summarized in Table 1, a reaction pH of 11.5 was identified as the optimal pH for producing PDA with a diameter of approximately 65 nm.

Table 1 The Diameter and PDI of PDA Synthesized in Different Reaction pH

pH	Eff. Diameter (nm)	PDI
8	351.2 ± 10.3	0.19 ± 0.021
9	328.8 ± 3.0	0.27 ± 0.0063
10	157.5 ± 2.5	0.10 ± 0.056
11	93.1 ± 6.3	0.18 ± 0.022
11.5	65.5 ± 2.8	0.16 ± 0.020
12	–	–

Effect of Reaction Temperature

As shown in Table 2, when the reaction pH was fixed at 11.5 and the reaction duration was maintained at 2 h, the size of the synthesized PDA gradually decreased with increasing reaction temperature. At 25°C, the hydrodynamic diameter of PDA was approximately 120 nm. When the temperature was raised to 37°C, the particle size decreased to approximately 66 nm. Further increasing temperature to 50°C yielded particles of 50 nm. However, these NPs exhibited a significantly higher polydispersity index (PDI). Consequently, the condition of 37°C was identified as optimal, producing PDA with a hydrodynamic diameter of approximately 65 nm and a narrow size distribution.

Effect of Reaction Time

When the reaction pH fixed at 11.5 and the temperature maintained at 37 °C, the particle size of PDA increased progressively with longer reaction times. As summarized in Table 3, the particle sizes obtained after 1 and 2 h of reaction were comparable at approximately 60 nm. However, the 2 h reaction yielded a higher quantity of NPs compared to the 1 h reaction. When the reaction time was extended to 4 and 12 h, the resulting PDA sizes increased to approximately 100 and 160 nm, respectively. Therefore, a reaction time of 2 h was determined to be optimal, providing a favorable balance between particle size and yield.

PDA was synthesized via the self-polymerization of dopamine hydrochloride under alkaline conditions in a Tris buffer system using a fixed dopamine hydrochloride concentration of 1 mg/mL. The optimized synthesis parameters were established as follows: reaction pH of 11.5, temperature, 37°C; and duration, 2 h. This specific combination of conditions yielded PDA with optimal hydrodynamic diameter and PDI profile.

Table 2 The Diameter and PDI of PDA Synthesized in Different Reaction Temperature

Temperature (°C)	Eff. Diameter (nm)	PDI
25	125.1 ± 1.5	0.18 ± 0.016
37	66.9 ± 2.7	0.31 ± 0.017
50	51.3 ± 5.3	0.73 ± 0.064

Table 3 The Diameter and PDI of PDA Synthesized in Different Reaction Time

Time	Eff. Diameter (nm)	PDI
1	59.5 ± 1.3	0.15 ± 0.042
2	64.4 ± 3.3	0.17 ± 0.038
4	99.7 ± 1.5	0.07 ± 0.029
12	162.9 ± 7.2	0.12 ± 0.034

https://doi.org/10.2147/IJN.S581479

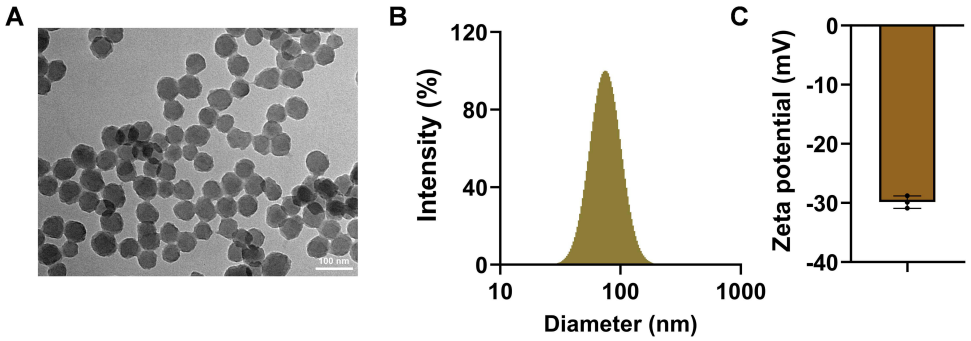

Figure 2 The characterization of synthetized PDA. (**A**) The TEM image of PDA, scale bar, 100 nm. (**B**) The particle size of PDA via DLS analysis. (**C**) The zeta potential of PDA, n = 3.

Characterization and Quantification of PDA

TEM imaging confirmed that the synthesized PDA had a monodisperse spherical morphology, with an average diameter of about 60 nm. Dynamic light scattering (DLS) measurements yielded a hydrodynamic diameter of approximately 70 nm, which was consistent with the TEM results and indicated a narrow size distribution. The zeta potential was −29.8 ± 1.1 mV (Figure 2). For accurate quantification, a standard curve was established by correlating the absorbance of serially diluted PDA solutions with the mass of lyophilized NPs (Table 4), resulting in a linear equation y = 1.1896x − 0.001 with a correlation coefficient (R^2) of 0.9999, demonstrating an excellent linear relationship.

Cellular Biocompatibility and Uptake Behavior of NPs

Prior to the functional evaluation, the cellular biocompatibility and internalization characteristics of the NPs were investigated. The viability of PC-12 cells after co-culture with varying concentrations of PDA was assessed via MTT assay. The results demonstrated that even at a high PDA concentration of 400 μg/mL and an extended incubation period of 48 h, the cell viability remained above 90%. No significant cytotoxicity was observed in any of the treatment groups, indicating excellent biocompatibility (Figure 3A). Furthermore, the uptake of PDA by PC-12 cells was quantitatively analyzed via flow cytometry at 1, 2, 4, and 8 h. The data revealed a gradual increase in fluorescence intensity over time, suggesting a time-dependent cellular uptake pattern, where internalization efficiency was positively correlated with incubation duration (Figure 3B).

ROS Scavenging Capacity

We further investigated the protective effects of PDA against ROS-induced damage at cellular level. PC-12 cells were pretreated with TBH to simulate oxidative stress. TBH treatment increased the percentage of ROS-positive cells from 0.19% to 94.01%. In contrast, subsequent PDA treatment significantly reduced the proportion of ROS-positive cells to 35.48%. Notably, PDA mitigated TBH-induced ROS elevation and substantially lowered basal ROS levels in the control cells (Figure 4). Consistent conclusions were drawn from the fluorescence microscopy images of the treated cells () Figure 5.

Concurrently, we observed and recorded cell morphology using bright-field microscopy. As shown in Figure 6, PC-12 cells exhibited marked morphological changes after 2 h of TBH treatment, including cell rounding and detachment, which were the characteristic features of cell death. In contrast, the PDA-treated cells demonstrated significant resistance to such damage, maintaining a normal morphology without evident rounding or detachment. The cellular morphology in

Table 4 Absorbance of Different Concentrations of PDA at 450 nm

Concentration (μg/mL)	0.0186	0.0373	0.0625	0.125	0.250	0.500	1.000
Absorbance	0.022	0.035	0.079	0.147	0.302	0.590	1.189

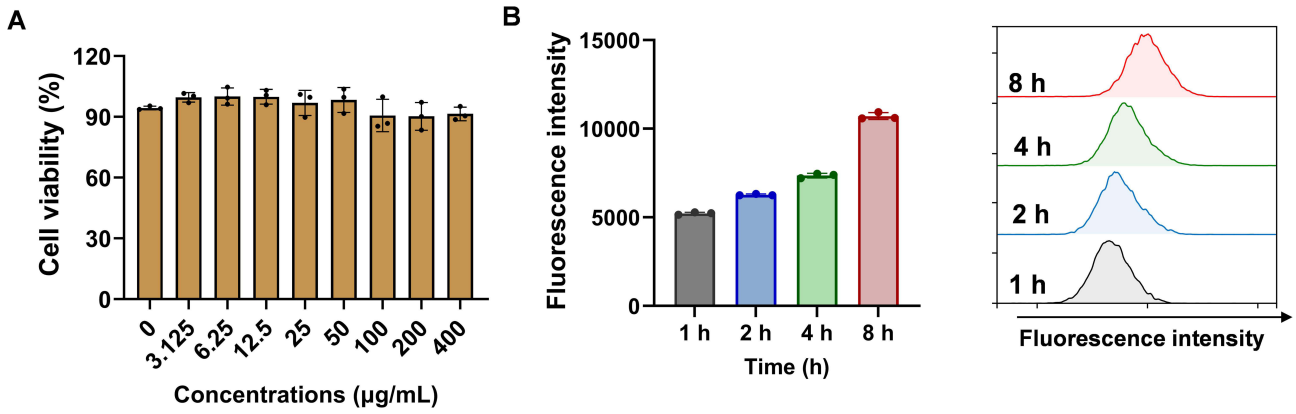

Figure 3 (**A**) Cell viability of PC-12 cells after incubation with PDA for 48 h, n = 3. (**B**) Cellular uptake of PDA by PC-12 cells. Representative histograms are shown on the right, n = 3.

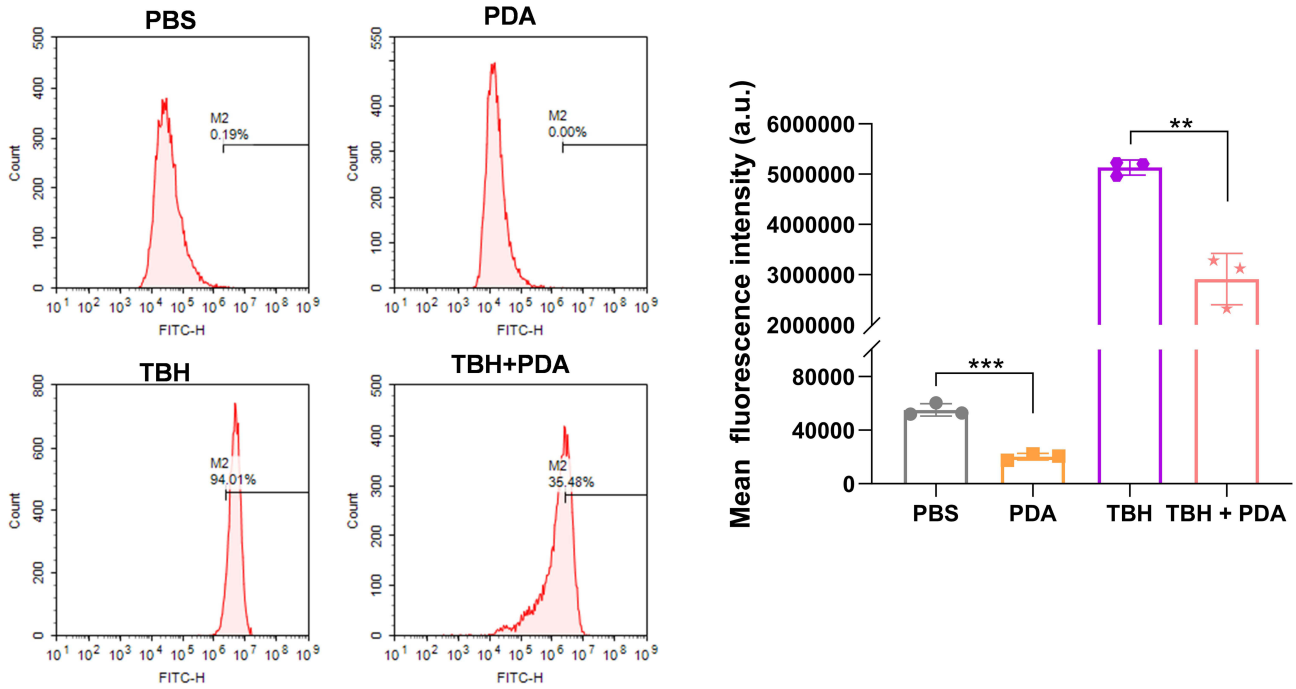

Figure 4 Flow cytometry measurement of the intracellular level of ROS. Representative flow cytometry plots of ROS levels are showing on the left. Data are expressed as mean ± SD, and significance defined as **P<0.05, **P<0.01, ***P<0.001*, n = 3.

the TBH+PDA group closely resembled that of the PBS group. In summary, PDA acts as an efficient ROS scavenger with a promising neuroprotective potential.

Effects of NPs on Microglial Polarization

Microglia can polarize into either a protective M2 phenotype or a neurotoxic M1 phenotype within the neuroinflammatory milieu.[23–25] The onset of neuroinflammation is frequently accompanied by microglial dysfunction,[4] and ameliorating the inflammatory microenvironment can help restore their homeostatic function.[26,27] To investigate whether PDA could promote microglial polarization toward the M2 phenotype, we first established an in vitro inflammation model by treating BV2 cells with TBH for 24 h. Flow cytometric analysis revealed a significant increase in the expression of the M1 marker CD86 in BV2 cells following TBH treatment, indicating the successful induction of M1 polarization and functional impairment under inflammatory conditions. Further assessment demonstrated that PDA treatment not only suppressed the activation of M1

https://doi.org/10.2147/IJN.S581479

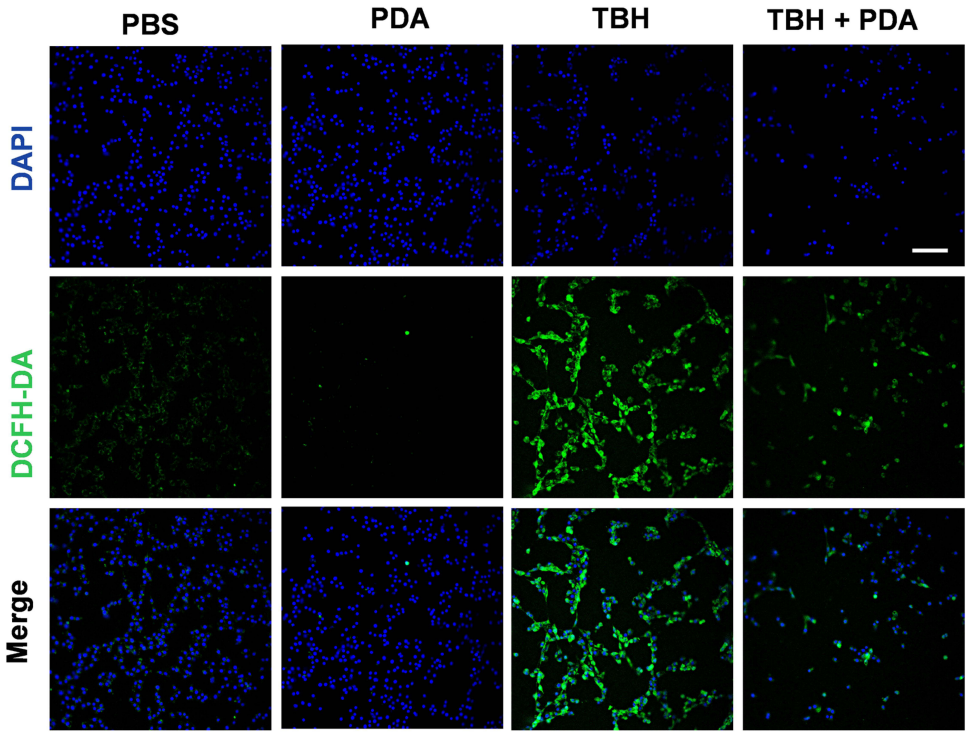

Figure 5 The fluorescence images of intracellular level of ROS, scale bar, 100 μm.

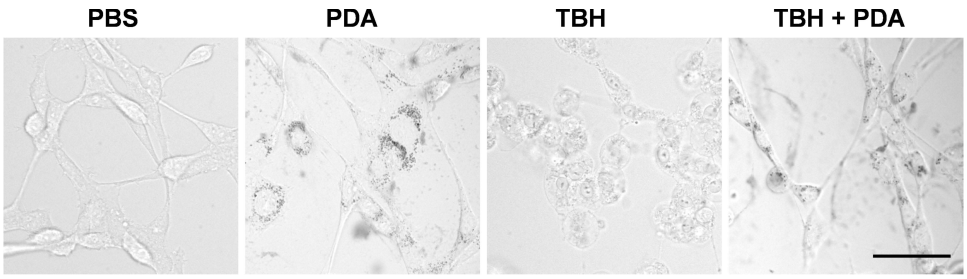

Figure 6 Changes in cell morphology after 2 h of TBH treatment in the presence and absence of PDA, scale bar, 50 μm.

microglia, as evidenced by the reduced CD86 expression, but also concurrently promoted M2 polarization, as indicated by the upregulated expression of the anti-inflammatory marker CD206 (Figure 7). These findings suggest that PDA have the potential to redirect microglial polarization from a pro-inflammatory to an anti-inflammatory phenotype.

Discussion

This study established a robust method for the size-controlled synthesis of PDA and demonstrated their dual neuroprotective functions via a combined antioxidant and immunomodulatory mechanism. Our optimized synthesis protocol, yielding monodisperse NPs around 60 nm, directly addressed a key bottleneck in the biomedical application of PDA. This size range was strategically selected based on evidence suggesting its optimal balance between systemic circulation and enhanced potential for BBB penetration.[20,22,28] The synthesized NPs exhibited potent ROS-scavenging capacity, effectively protecting neuronal cells from oxidative insult. This activity was directly attributable to the catechol-rich structure of PDA, which acted as a redox-active moiety.[29] More significantly, our data revealed the ability of PDA to reprogram microglial polarization from a pro-inflammatory M1 state toward a protective M2 phenotype. This shift was critical, as chronic M1 activation is a major driver of neuroinflammation and secondary neuronal damage in neurodegenerative diseases.[4] Our findings suggested that PDA can intervene not only at the level of the initial oxidative trigger but also in the subsequent inflammatory cascade. The

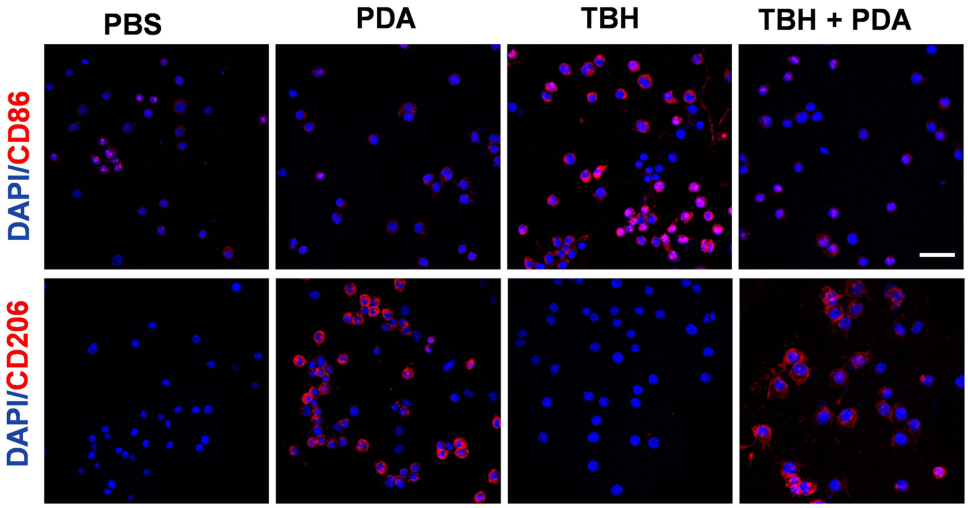

Figure 7 Fluorescence images for CD86 and CD206 expression analysis, scale bar, 50 μm.

functionality of PDA likely disrupted the self-perpetuating cycle of oxidative stress and neuroinflammation. While the exact signaling pathways through which PDA modulate microglial polarization require further elucidation, their surface chemistry and potential interactions with key receptors involved in immune regulation warrant investigation.

While methodologies for the size-tunable synthesis of PDA via alkaline polymerization were established,[30] their optimization for specific biomedical applications required distinct functional targets. The development of neuroprotective nanotherapeutics demands a focus on different priorities: efficient potential for brain entry, optimal neuronal and microglial cell uptake, and the ability to disrupt the interconnected pathologies of oxidative stress and neuroinflammation characteristic of neurodegenerative diseases. Therefore, systematically optimizing PDA size specifically for neuroprotection, particularly within the sub-100 nm range critical for brain delivery, and elucidating their impact on integrated antioxidant and immunomodulatory functions in neural cell models, represented a distinct and necessary advancement. This study was designed to address this specific issue.

Compared to other antioxidant nanoformulations, PDA offer distinct benefits, including straightforward, catalyst-free synthesis and inherent biocompatibility. Their surface-adherent properties also provide a versatile platform for further functionalization with targeting ligands or therapeutic cargos, potentially enhancing their specificity and efficacy.[31,32] However, several challenges remain for clinical translation. Future work must include comprehensive in vivo studies to confirm long-term biodistribution and safety profiles in relevant animal models. The biodegradation kinetics and clearance pathways of PDA also need detailed characterization.

Conclusions

In summary, this study established a method for the controlled preparation of PDA by precisely regulating the key alkaline synthesis parameters. The optimized NPs exhibited a uniform size distribution and demonstrated neuroprotective functions through effective ROS scavenging and induction of microglial polarization toward the anti-inflammatory M2 phenotype. These findings revealed a coordinated mechanism of antioxidant activity and immunomodulation, providing a solid foundation for the development of PDA-based neuroprotective nanotherapeutics.

Acknowledgments

This study was supported by the 2025 General Scientific Research Project of Shaanxi Provincial Education Department (NO. 25JK0424).

Author Contributions

All authors made a significant contribution to the work reported, whether that is in the conception, study design, execution, acquisition of data, analysis and interpretation, or in all these areas; took part in drafting, revising or critically

reviewing the article; gave final approval of the version to be published; have agreed on the journal to which the article has been submitted; and agree to be accountable for all aspects of the work.

Disclosure

The authors report no conflicts of interest in this work.

References

1. Dash UC, Bhol NK, Swain SK, et al. Oxidative stress and inflammation in the pathogenesis of neurological disorders: mechanisms and implications. *Acta Pharm Sin B*. 2025;15(1):15–34. doi:10.1016/j.apsb.2024.10.004
2. Wilson DM 3rd, Cookson MR, Van Den Bosch L, Zetterberg H, Holtzman DM, Dewachter I. Hallmarks of neurodegenerative diseases. *Cell*. 2023;186(4):693–714. doi:10.1016/j.cell.2022.12.032
3. Peruzzotti-Jametti L, Willis CM, Krzak G, et al. Mitochondrial complex I activity in microglia sustains neuroinflammation. *Nature*. 2024;628 (8006):195–203. doi:10.1038/s41586-024-07167-9
4. Shi FD, Yong VW. Neuroinflammation across neurological diseases. *Science*. 2025;388(6753):eadx0043. doi:10.1126/science.adx0043
5. He W, Liu M, Zhang T, et al. Tannic acid-iron complex-based nanozyme ameliorates parkinson's disease via relieving oxidative stress and neuroinflammation. *ACS Nano*. 2025;19(37):33212–33229. doi:10.1021/acsnano.5c07601
6. Huang J, Wu F, Cao W, et al. Ultrasmall iron-gallic acid coordination polymer nanoparticles for scavenging ROS and suppressing inflammation in tauopathy-induced Alzheimer's disease. *Biomaterials*. 2025;317:123042. doi:10.1016/j.biomaterials.2024.123042
7. Niu X, Gao B, Huang H, et al. Carbon monoxide nanomodulator reverses ischemia-reperfusion injury in stroke: a novel dual-channel therapy mode of co-driving neuroprotection and neurogenesis. *Adv Sci*. 2025;13:e12333. doi:10.1002/advs.202512333
8. Gao J, Xia Z, Gunasekar S, Jiang C, Karp JM, Joshi N. Precision drug delivery to the central nervous system using engineered nanoparticles. *Nature Rev Mater*. 2024;9(8):567–588.
9. Cheng W, Zeng X, Chen H, et al. Versatile polydopamine platforms: synthesis and promising applications for surface modification and advanced nanomedicine. *ACS Nano*. 2019;13(8):8537–8565. doi:10.1021/acsnano.9b04436
10. Qi C, Fu L-H, Xu H, Wang T-F, Lin J, Huang P. Melanin/polydopamine-based nanomaterials for biomedical applications. *Sci China Chem*. 2019;62 (2):162–188. doi:10.1007/s11426-018-9392-6
11. Geng R, Xiao W, Bi D, et al. Heat-responsive phase-change cream broadly enhances transdermal delivery through a mild photothermal strategy. *Adv Mater*. 2025;38:e16017. doi:10.1002/adma.202416017
12. Li G, Wei X, Lv K, et al. Cyclodextrin-based self-assembling hydrogel for Photothermal-controlled nitric oxide release in stage-specific treatment of MRSA-induced arthritis. *Carbohydr Polym*. 2025;359:123578. doi:10.1016/j.carbpol.2025.123578
13. Chen H, Zhang H, Li J, et al. Polydopamine nanohydrogel decorated adhesive and responsive hierarchical microcarriers for deafness protection. *Adv Sci*. 2025;12(29):e2407637. doi:10.1002/advs.202407637
14. Zhang L, Du H, Sun X, et al. 3D printing of interpenetrating network flexible hydrogels with enhancement of adhesiveness. *ACS Appl Mater Interfaces*. 2023;15(35):41892–41905. doi:10.1021/acsami.3c07816
15. Park J, Brust TF, Lee HJ, Lee SC, Watts VJ, Yeo Y. Polydopamine-based simple and versatile surface modification of polymeric nano drug carriers. *ACS Nano*. 2014;8(4):3347–3356. doi:10.1021/nn405809c
16. Ding Z, Bao X, Zhao Y, et al. Polydopamine nanodots ameliorate inflammatory bowel disease by restoring redox homeostasis and intestinal microenvironment. *Adv Sci*. 2025;12(47):e08674. doi:10.1002/advs.202508674
17. Jiang C, Yang X, Huang Q, et al. Microglial-biomimetic memantine-loaded polydopamine nanomedicines for alleviating depression. *Adv Mater*. 2025;37(9):e2417869. doi:10.1002/adma.202417869
18. Yin N, Zhang Z, Ge Y, et al. Polydopamine-based nanomedicines for efficient antiviral and secondary injury protection therapy. *Sci Adv*. 2023;9 (24):eadf4098. doi:10.1126/sciadv.adf4098
19. Li B, Ma L, Li X, et al. Size matters: altering antigen specific immune tolerance by tuning size of particles. *J Control Release*. 2024;373:823–836. doi:10.1016/j.jconrel.2024.07.077
20. Xu M, Qi Y, Liu G, Song Y, Jiang X, Du B. Size-dependent in vivo transport of nanoparticles: implications for delivery, targeting, and clearance. *ACS Nano*. 2023;17(21):20825–20849. doi:10.1021/acsnano.3c05853
21. Guo H, Wei Z, Zhou H, et al. Microinvasive deployment and fate-determination of functional, engineered nanoparticles in central nervous system. *ACS Mater Lett*. 2025;7(6):2288–2309. doi:10.1021/acsmaterialslett.5c00698
22. Asimakidou E, Tan JKS, Zeng J, Lo CH. Blood-brain barrier-targeting nanoparticles: biomaterial properties and biomedical applications in translational neuroscience. *Pharmaceuticals*. 2024;17(5). doi:10.3390/ph17050612
23. Depp C, Doman JL, Hingerl M, Xia J, Stevens B. Microglia transcriptional states and their functional significance: context drives diversity. *Immunity*. 2025;58(5):1052–1067. doi:10.1016/j.immuni.2025.04.009
24. Gao C, Jiang J, Tan Y, Chen S. Microglia in neurodegenerative diseases: mechanism and potential therapeutic targets. *Signal Transduct Target Ther*. 2023;8(1):359. doi:10.1038/s41392-023-01588-0
25. Guo S, Wang H, Yin Y. Microglia polarization from M1 to M2 in neurodegenerative diseases. *Front Aging Neurosci*. 2022;14:815347. doi:10.3389/fnagi.2022.815347
26. Feng Q, Zhang X, Zhao X, et al. Intranasal delivery of pure nanodrug loaded liposomes for alzheimer's disease treatment by efficiently regulating microglial polarization. *Small*. 2024;20(50):e2405781. doi:10.1002/smll.202405781
27. Yin N, Zhao Y, Liu C, et al. Engineered nanoerythrocytes alleviate central nervous system inflammation by regulating the polarization of inflammatory microglia. *Adv Mater*. 2022;34(27):e2201322. doi:10.1002/adma.202201322
28. Huo S, Ma H, Huang K, et al. Superior penetration and retention behavior of 50 nm gold nanoparticles in tumors. *Cancer Res*. 2013;73(1):319–330. doi:10.1158/0008-5472.CAN-12-2071

29. Guo Y, Baschieri A, Mollica F, et al. Hydrogen atom transfer from HOO(.) to ortho-Quinones explains the antioxidant activity of polydopamine. *Angew Chem Int Ed Engl*. 2021;60(28):15220–15224. doi:10.1002/anie.202101033
30. Carmignani A, Battaglini M, Sinibaldi E, et al. In vitro and ex vivo investigation of the effects of polydopamine nanoparticle size on their antioxidant and photothermal properties: implications for biomedical applications. *ACS Appl Nano Mater*. 2022;5(1):1702–1713. doi:10.1021/acsanm.1c04536
31. Zhou X, Wang L, Wu Y, et al. Bioactive polydopamine nanomedicines-assisted cancer immunotherapy. *Mater Today Bio*. 2025;32:101864. doi:10.1016/j.mtbio.2025.101864
32. Yang F, Dai L, Shi K, et al. A facile boronophenylalanine modified polydopamine dual drug-loaded nanoparticles for enhanced anti-tumor immune response in hepatocellular carcinoma comprehensive treatment. *Biomaterials*. 2024;305:122435. doi:10.1016/j.biomaterials.2023.122435